



# Incorporating buckling effect into the topology design of 2D continuum structures using isolines

Mariano Victoria<sup>a,\*</sup>, Concepción Díaz<sup>a</sup>, Pascual Martí<sup>a</sup>, Osvaldo M. Querín<sup>b</sup>

<sup>a</sup> Department of Structures, Construction and Graphical Expression, Technical University of Cartagena, Cartagena, Spain

<sup>b</sup> School of Mechanical Engineering, University of Leeds, Leeds, United Kingdom

## ARTICLE INFO

### Keywords:

Topology design  
Buckling  
Continuum structures  
Isolines  
Fixed grid

## ABSTRACT

Isolines Topology Design (ITD) is an iterative algorithm for use in the topological design of two-dimensional (2D) continuum structures using isolines. This paper presents an extension to this algorithm for topology design of 2D continuum structures under the influence of buckling. Topology design has been used to obtain the lightest structure that can support the loading conditions without failure, with optimal designs typically consisting of slender members. In many cases, instability (or buckling) of the slender compressive members may occur at load levels below those predicted using a stress-based failure criteria. Although topology optimization is often used in the conceptual phase of the design, the influence of buckling has a significant impact on the features and performance of the final structure. This article presents an alternative approach to incorporate the buckling effect into the ITD algorithm for the design of 2D continuum structures. The concept consists of transforming the buckling topology optimization problem into a conventional von Mises stress-based topology design problem at each iteration using the shape of the buckling mode of the structure obtained by the eigenvalue analysis. Three examples are presented to show the viability and effectiveness of the alternative approach implemented into the ITD algorithm. The effect of the displacement factor ratio value on the first critical load of a resulting design was studied. The resulting designs presented are in good agreement with those from the literature. The main conclusion is that the alternative approach can maximize the first critical load of a design subject to final volume constraints if the associated stiffness loss can be assumed.

## 1. Introduction

The topology optimization (TO) problem is normally formulated in terms of compliance minimization (Ooms et al. (2023) [1]), which is an important parameter of structural performance. However, lightweight, sparse, or slender structures are characterized by multiple objectives or constraints, and several aspects must be considered in their designs, such as: strength (Wang et al. (2022) [2]), natural frequency (Zhang et al. (2020) [3]), stability (Hajlaoui et al. (2021) [4], Liang and Li (2022) [5], Ngoc et al. (2022) [6], Guo et al. (2022) [7], Jiang et al. (2023) [8]), manufacturing requirements (Ebeling-Rump et al. (2021) [9]), uncertainties (Li et al. (2022) [10], Li et al. (2023) [11]), etc.

Generally, the purpose of structural optimization is to obtain the lightest structure that can support the loading conditions without failure. Minimum weight structures typically consist of slender members (trust- or beam-like elements) or thin panels which are subjected to uniaxial tensile or compressive loads. In many cases, instability (or

buckling) of the slender compressive members may occur at load levels below those predicted by the stress-based failure criteria. This limits the capacity of the structure to carry the load and may affect its safety.

Buckling TO (BTO) consists of obtaining the optimal material layout of a structure that also considers the buckling effect. Although TO is often used in the conceptual phase of the design, the influence of buckling has a significant impact on the features and performance of the final structure. Compared to conventional TO, BTO is more computationally expensive, mainly due to the calculation of the buckling loads at each optimization iteration.

Large-scale engineering structures, such as bridges, electric transmission towers, high-rise buildings, giant boom cranes, etc., are often made from slender members in such a way that the volume of material in the optimal structure consists of only a very small fraction of the total volume of the original design domain. These optimal light and sparse structures require just the right amount of material for load support which generally makes their components slender and consequently

\* Corresponding author.

E-mail address: [mariano.victoria@upct.es](mailto:mariano.victoria@upct.es) (M. Victoria).

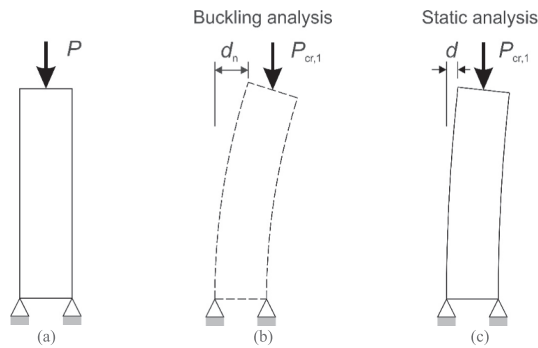


**Fig. 1.** Schematic view of procedure to incorporate the buckling effect into the optimization process: (a) Original structure with applied load; (b) Buckled structure showing the magnitude of the critical load ( $P_{cr,1}$ ) and displacement vector ( $d_n$ ); (c) New modified geometry of the structure with applied critical load ready for topology optimization.

more prone to buckling. The buckling phenomenon is a crucial factor that may define the safety level of a structure. Due in part to this, buckling topology optimization has attracted more attention in recent years.

Buckling has been considered in both truss and continuum TO. For truss TO, the design space typically consists of a fixed set of nodes connected by many pin-jointed truss members, known as a ground structure. Member cross-sections are usually the design variables, which can be reduced to zero to allow a change in topology. Local Euler buckling constraints can be specified on each member, although a modification of the design space is often required to handle discontinuities when member areas are reduced to zero (Rozvany (1996) [12]). For continuum structures, it can be difficult to consider local buckling behaviours with Euler-type constraints, since it is very difficult to identify discrete structural members, their geometrical properties, and their end support conditions (Rahmatalla and Swan (2003) [13]).

Considerable efforts have been made in the last 20 years to develop methods to solve the optimization problem considering the buckling effect. Buckling optimization of continuum structures has attracted considerable attention in recent years, being an active and challenging research area.

Rahmatalla and Swan (2003) [13] proposed a continuum topology optimization methodology suitable for finding optimal forms of large-scale sparse structures. Since the need to avoid long compressive spans can be critical in determining the optimal form of such structures, a formulation was used in which the structure was modelled as a linear elastic continuum subjected to design loads and optimized to maximize the minimum critical buckling load.

Kemmler et al. (2005) [14] focused on large deformations and stability in topology optimization. The instability condition was incorporated into the design process as an inequality constraint with the critical load level determined directly. To reduce the imperfection sensitivity, a geometrically modified structure was also introduced which included the imperfection shape.

Browne et al. (2012) [15] proposed a method to find solutions of large-scale binary programming problems where the calculation of derivatives is very expensive. The method was applied to a weight minimization TO problem with compliance and buckling constraints.

Bochenek and Tajs-Zielińska (2015) [16] introduced a new approach to the TO of columns against instability. The idea was to replace a conventional maximization of a buckling load by a locally formulated topology optimization problem based on compliance minimization.

Luo and Tong (2015) [17] investigated topology design optimization for maximizing critical buckling loads of thin-walled structures using a Moving Iso-Surface Threshold (MIST) method. Linear buckling optimization was conducted to maximize the critical buckling load factor for a thin-walled structure subjected to either compressive forces or prescribed compressive displacements.

Gao et al. (2017) [18] presented an adaptive continuation method for BTO of continuum structures using the Solid Isotropic Material with Penalization (SIMP) method. For optimization problems of minimizing

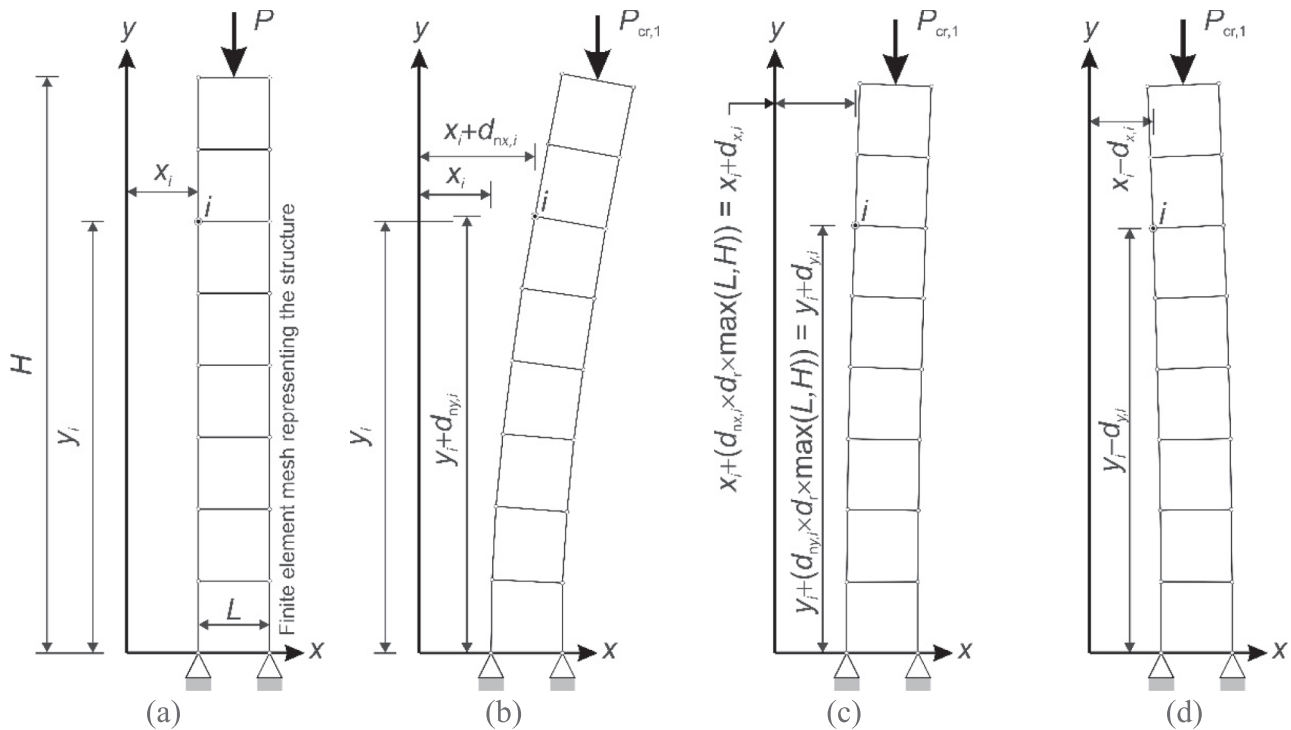


**Fig. 2.** Schematic view of the procedure to obtain the modified structural geometries. Node  $i$  location in: (a) Structure represented with eight finite elements; (b) Buckling mode shape; (c) Modified structural geometry with positive modification vector ( $d$ ); (d) Modified structural geometry with negative modification vector ( $-d$ ).

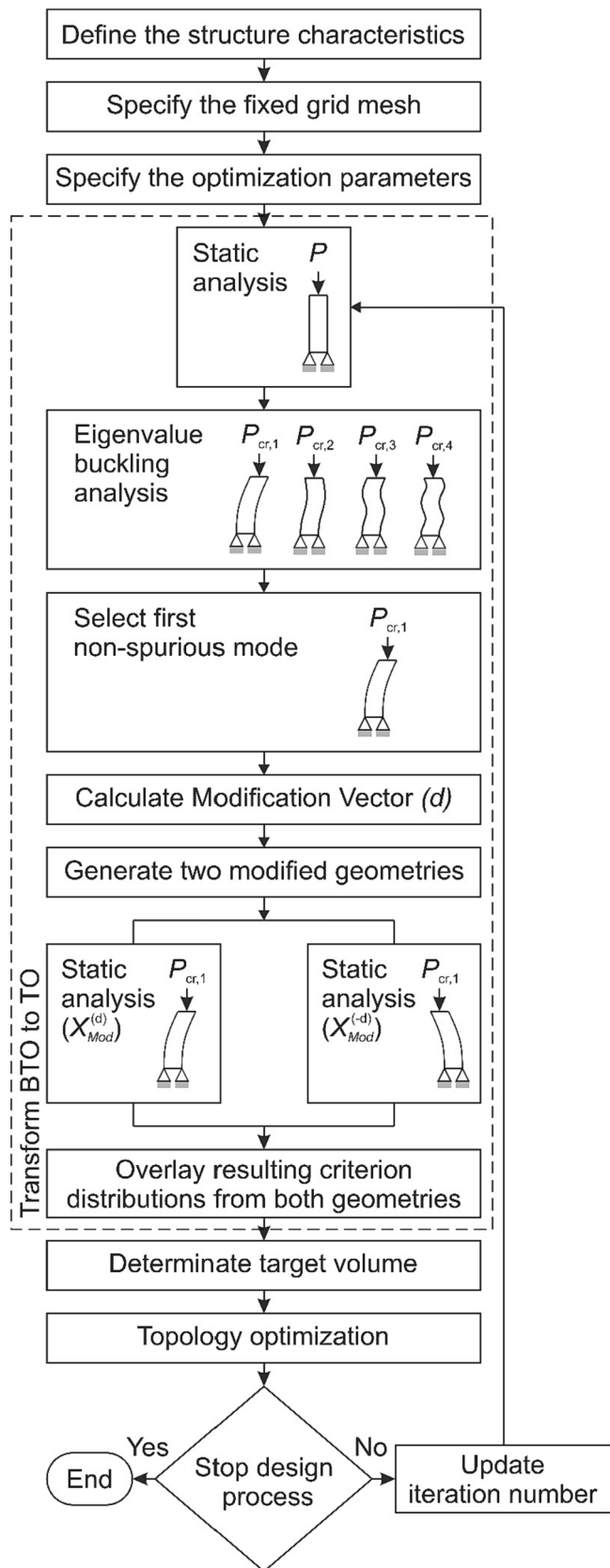


Fig. 3. Flow chart of modified ITD algorithm to carry out buckling topology optimization.

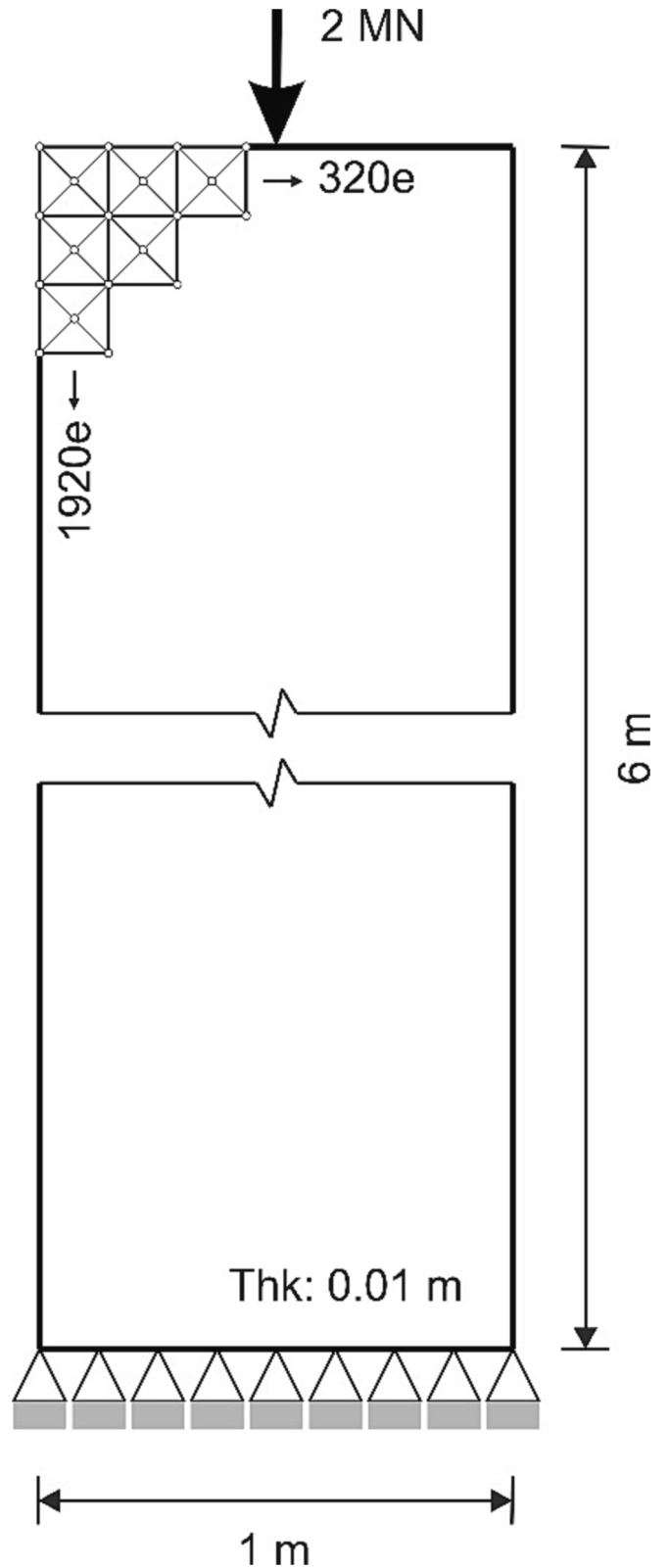
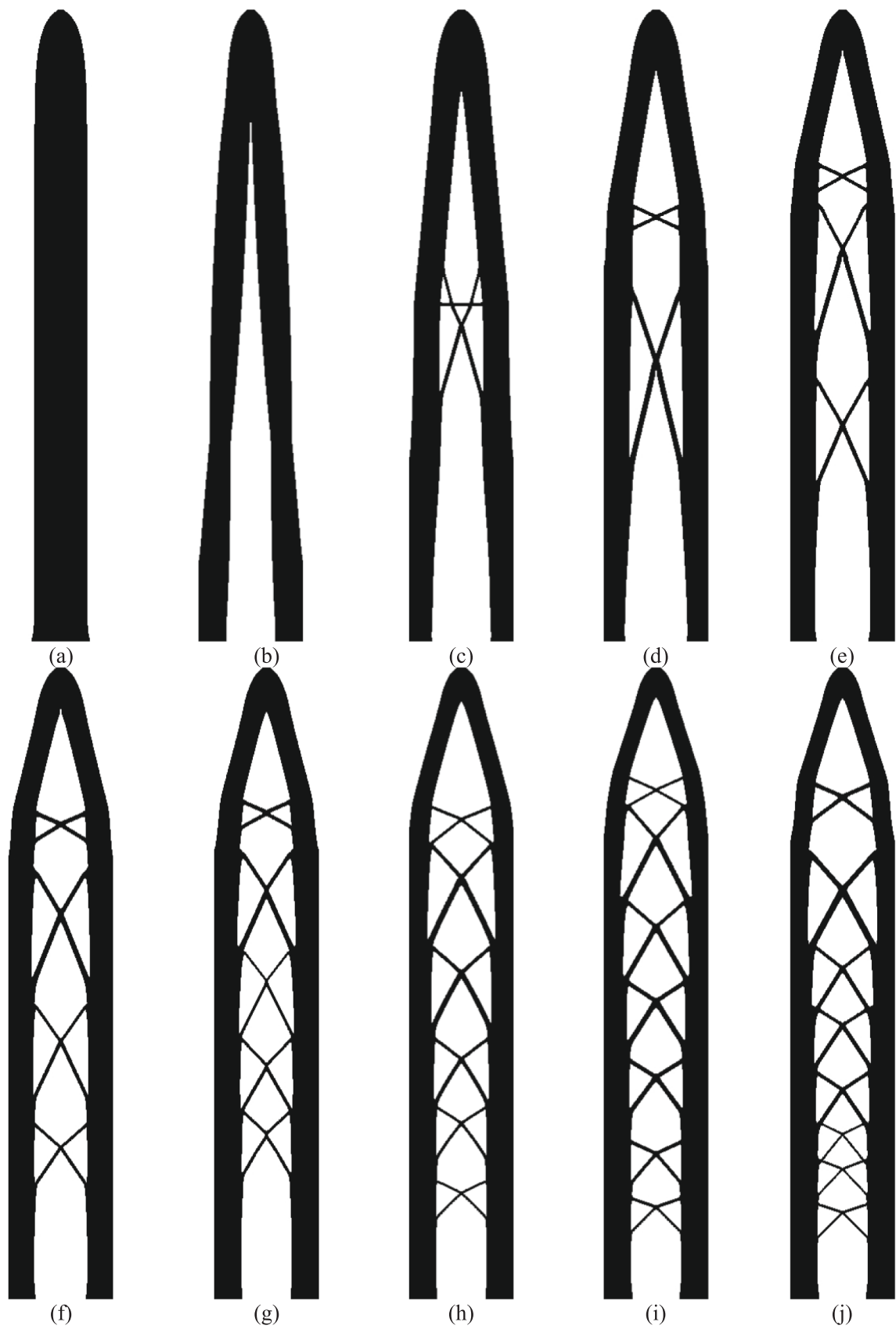


Fig. 4. Design domain for the clamped column loaded at the centre of the top edge.

structural compliance subjected to constraints on material volume and buckling load factors, it was found that the conflict between the structural stiffness and stability requirements may have an adverse impact on the performance of the optimization algorithms. An automatic scheme for adjusting the penalization parameter was introduced to address this



**Fig. 5.** Final designs for the clamped column for a volume fraction of  $V_f/V_0 = 0.5$ . Effect of different  $d_t$  values on the optimal design: (a) 0, (b) 0.01, (c) 0.025, (d) 0.05, (e) 0.1, (f) 0.125, (g) 0.15, (h) 0.2, (i) 0.25, (j) 0.3.

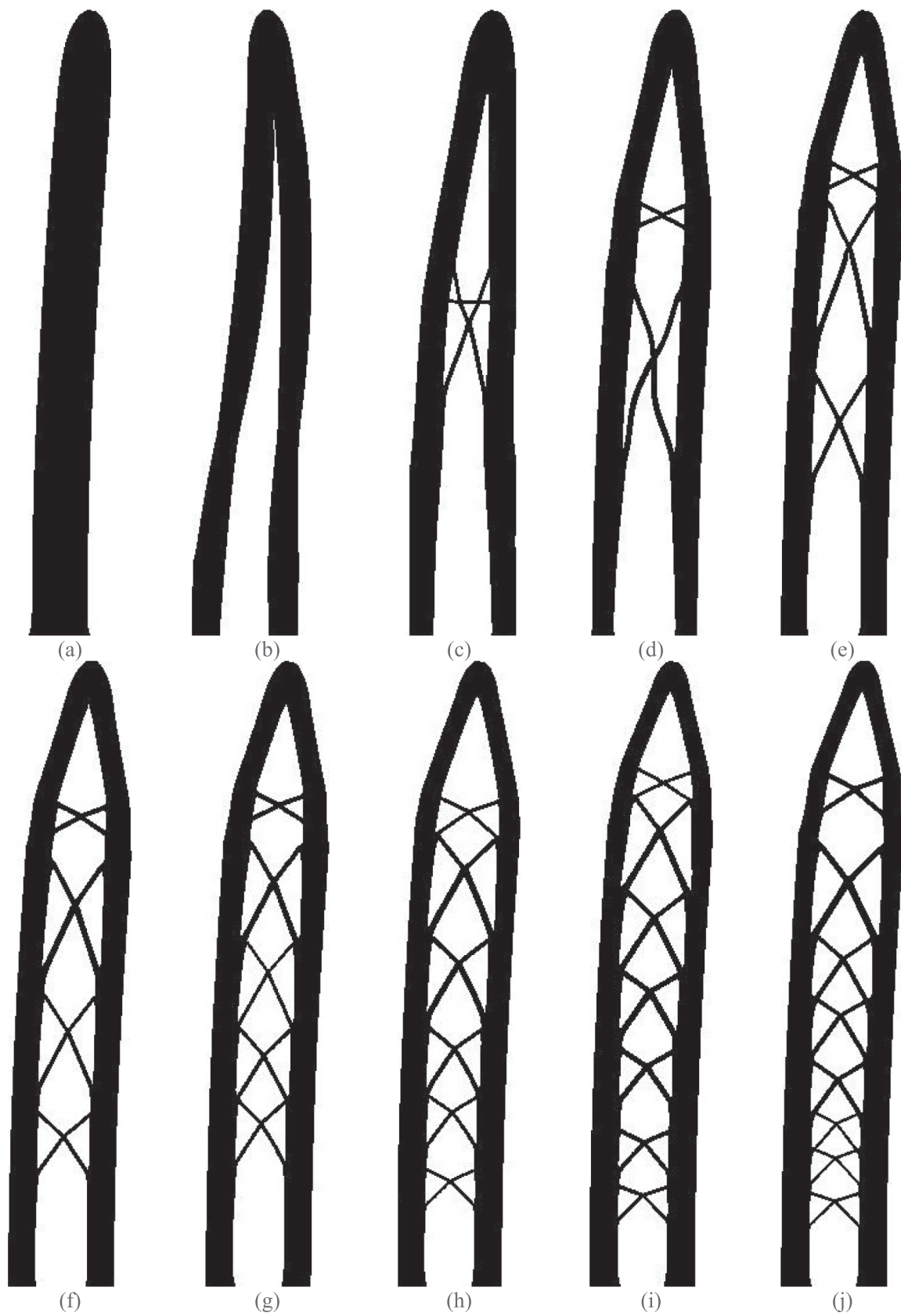
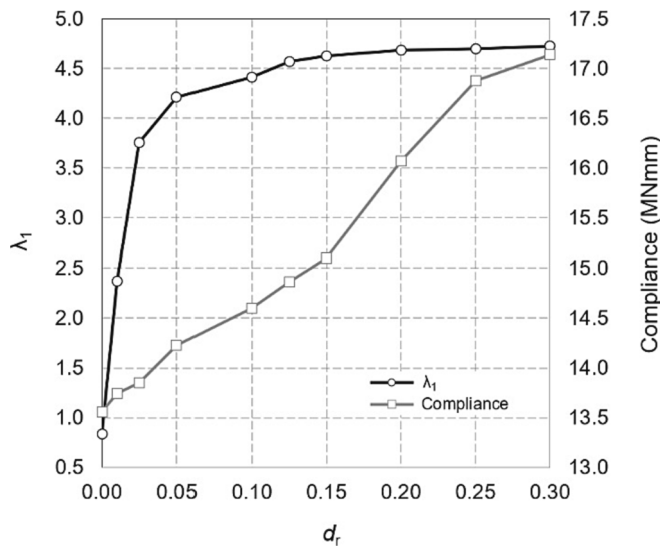


Fig. 6. First lowest buckling mode shapes for the optimal columns of Fig. 5 with  $d$  values of: (a) 0, (b) 0.01, (c) 0.025, (d) 0.05, (e) 0.1, (f) 0.125, (g) 0.15, (h) 0.2, (i) 0.25, (j) 0.3.

**Table 1**

Comparison of the first eigenvalue ( $\lambda_1$ ), maximum total displacement ( $d_{t,max}$ ) and compliance ( $C$ ) values for the optimal columns obtained for a volume fraction of  $V_f/V_0 = 0.5$  and different  $d_r$  values.

ANSYS	Eigenvalue analysis		Static analysis	
	$\lambda_1$	$d_{t,max}$ (mm)	$d_{t,max}$ (mm)	$C$ (MNmm)
Initial	5.906	8.484	8.484	8.484
0.000	0.837	13.56	13.56	13.56
0.010	2.371	13.74	13.74	13.74
0.025	3.757	13.85	13.85	13.85
0.050	4.215	14.24	14.24	14.24
0.100	4.409	14.62	14.62	14.62
0.125	4.569	14.99	14.99	14.99
0.150	4.626	15.11	15.11	15.11
0.200	4.682	16.07	16.07	16.07
0.250	4.700	16.89	16.89	16.89
0.300	4.726	17.13	17.13	17.13



**Fig. 7.** Plot of the first eigenvalue and compliance versus displacement factor ratio for the optimal columns.

conflict and generate better designs.

Ferrari et al. (2018) [19] presented an efficient solution method for structural topology optimization aimed at maximizing the fundamental frequency of vibration. The proposed method relies on replacing the eigenvalue problem with a frequency response one, which can be tuned and efficiently solved by a multilevel procedure.

Townsend and Kim (2019) [20] applied the Level Set Method (LSM) to the buckling behaviour of shell structures. They used a sequential level set TO method that was shown to naturally avoid the issues related to mode ordering and if required, is capable of simultaneously increasing multiple buckling loads at once.

Dalklint et al. (2021) [21] demonstrated how a strain energy transition approach can be used to remove artificial buckling modes that often occur in stability constrained topology optimization problems.

Ferrari et al. (2021) [22] presented a 250-line Matlab code for topology optimization for linearized buckling criteria. The code was conceived to handle stiffness, volume and buckling load factors either as the objective function or as constraints. The efficiency and flexibility of the code were demonstrated over a few structural design examples.

Hajlaoui et al. (2021) [4] proposed in their work a simple and efficient solid shell element formulation using First-order Shear Deformation Theory (FSDT) and a special representation of transverse shear strains imposed on the strain-compatible part for thermal buckling analysis of Functionally Graded Material (FGM) shells.

Liang and Li (2022) [5] reformulated the Koiter-Newton method to

have the capability of the geometrically nonlinear thermal–mechanical buckling analysis. The biggest innovation of this contribution is the conversion of initial temperature effects to be an extra independent degree of freedom in the thermal–mechanical reduced-order model, by means of the novel Koiter theory.

Ngoc et al. (2022) [6] used an adaptive mapping technique to examine multiscale bucking optimal topology for structural coating. The Adaptive Geometric Components (AGCs) include a framework of macro-sandwich bars representing a macrostructure with a solid coating and a group of micro-solid bars representing the nonuniform concurrent at the microstructural scale.

Guo et al. (2022) [7] presented a new reliability-based topology optimization model under buckling and compliance constraints to deal with the uncertainties incurred by Young’s modulus and load variations, which aims to minimize the manufacturing cost under reliability and stability requirements. To combine the multiple constraints to a single smooth and differentiable constraint, a Kreisselmeier-Steinhauser aggregation function was used.

Jiang et al. (2023) [8] proposed an algorithm for topology optimization for minimum compliance with material volume and buckling constraints under design-dependent loads was developed. The structural topology optimization problem was solved using the SIMP method along with a pressure boundary searching scheme based on the Distance Regularized Level Set Evolution (DRLSE) model to deal with design-dependent loads.

The novelty of this work corresponds with extending the isolines topology design (ITD) algorithm of Victoria et al. (2009) [23], by incorporating a new approach that considers buckling effect into the design of two-dimensional (2D) continuum structures. This is achieved by transforming the buckling topology design problem into a stress-based design problem at each iteration using the shape of the buckling mode of the structure obtained by the eigenvalue analysis. Three examples are presented to show the viability and effectiveness of incorporating this approach into the ITD algorithm.

## 2. Fixed grid finite element analysis

The fixed grid (FG) finite element (FE) analysis (FEA) method of García-Ruiz and Steven (1999) [24] was used in this work. In FG-FEA, the elements are in a fixed position in space and have the real structure superimposed on them. This means that there are elements which lie inside (I), outside (O), or on the boundary (B) of the structure.

The elasticity modulus for O elements is given by Eq. (1)

$$E_O = E_I \times r_{fg} \tag{1}$$

where  $E_I$  is the elasticity modulus for an element inside, and  $r_{fg}$  is the fixed grid ratio. The value of  $E_O$  plays a crucial role to avoid the appearance of spurious modes. A large value  $r_{fg} > 10^{-3}$  can result in non-realistic high stiffness of void elements. Conversely, a small value of  $r_{fg} < 10^{-9}$  can be insufficient to avoid the issue of spurious modes (see Section 2.1) and introduces ill-conditioned problems in stiffness matrix (Zhou (2004) [25], Lindgaard and Dahl (2013) [26] and Gao and Ma (2015) [27]). So from the literature, appropriate fixed grid ratio values to use should be in the range:  $10^{-6} < r_{fg} < 10^{-3}$ .

The ANSYS program [28] was used to implement the FG method by using the PLANE182 FE. This element is defined by four- or three-nodes and has two translation degrees of freedom at each node. The element has plasticity, hyperelasticity, stress stiffening, large deflection, and large strain capabilities. The ANSYS keyoptions used were: enhanced strain formulation (to prevent shear locking in bending-dominated problems); plane stress with thickness; and pure displacement formulation. A full review of this element can be found in [28].

Although PLANE182 performance may be lower in comparison to other more sophisticated finite elements (e.g., PLANE183), it is compensated by its simplicity, computational cost, and adaptability

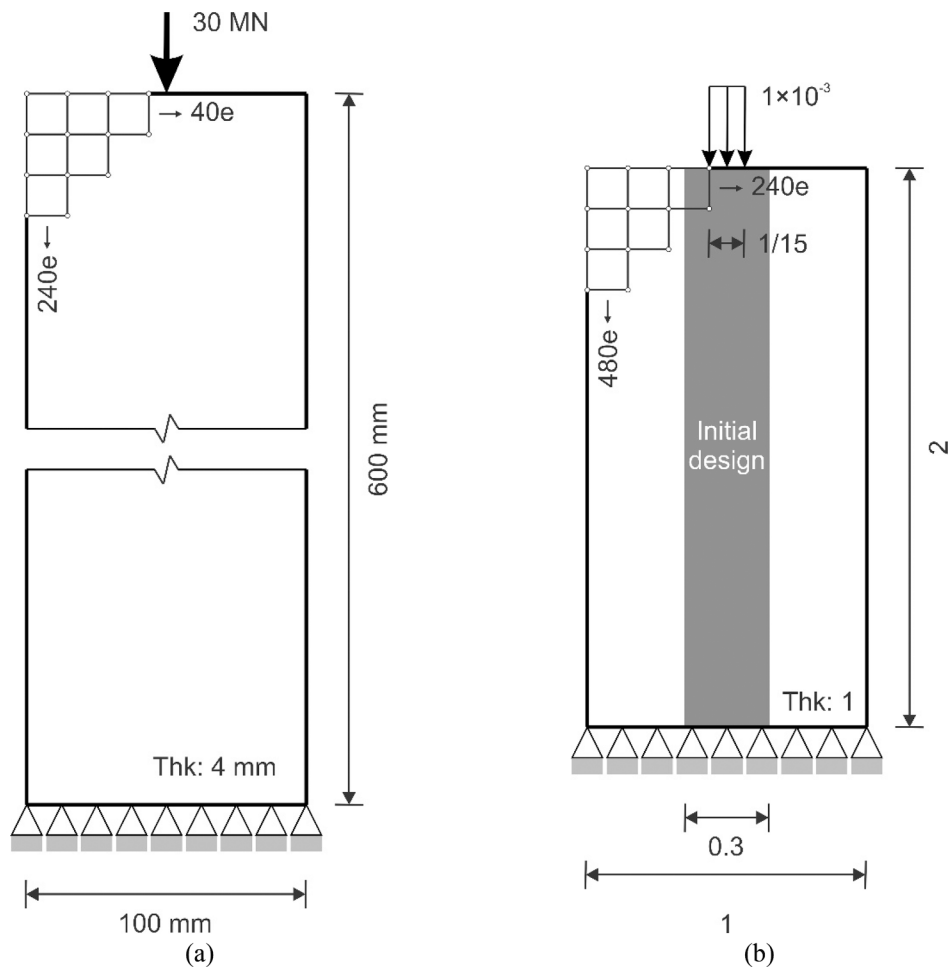


Fig. 8. Design domain for the clamped columns loaded in compression at the centre of the top edge: (a) Luo and Tong (2015) [17], (b) Ferrari et al. (2021) [22].

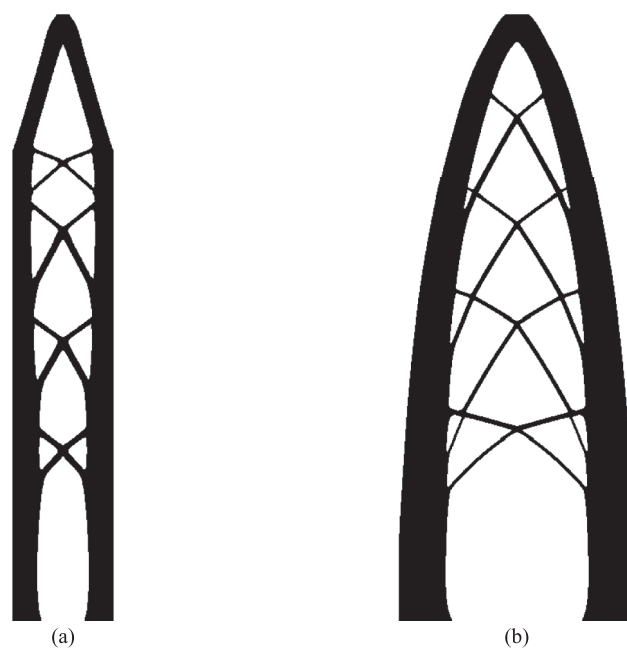


Fig. 9. Final column designs: (a) 6 by 1 for a volume fraction of  $V_f/V_0 = 0.5$ , (b) 2 by 1 for a volume fraction of  $V_f/V_0 = 0.25$  resulting from this work.

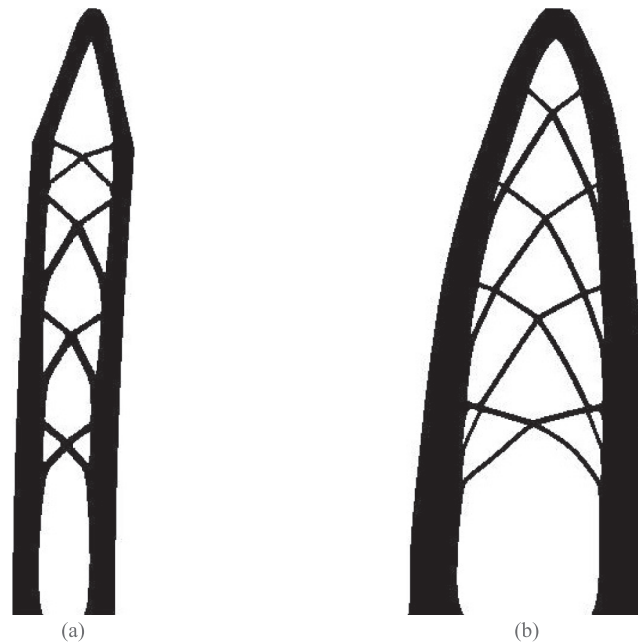


Fig. 10. First lowest buckling mode shapes for the optimal columns shown of Fig. 9: (a) 6 by 1 for a volume fraction of  $V_f/V_0 = 0.5$ , (b) 2 by 1 for a volume fraction of  $V_f/V_0 = 0.25$ .

Table 2  
Comparison of the first eigenvalue ( $\lambda_1$ ) for the columns of aspect ratio 6 and 2 by 1.

ANSYS Aspect ratio	Final volume fraction	$\lambda_1$ Initial	New approach	[17]	[22]
6 by 1	0.50	5.25	4.18	4.04	-
2 by 1	0.25	1.39	8.41	-	8.53

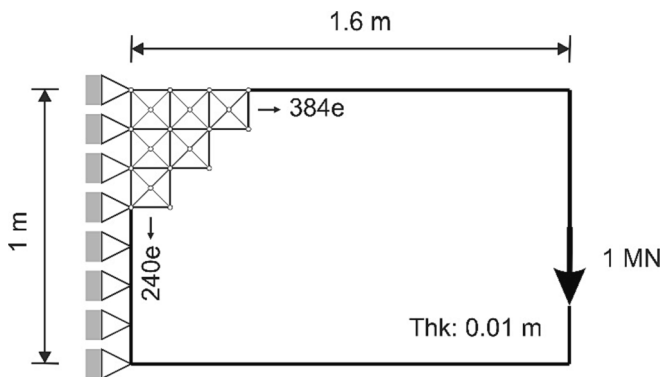


Fig. 11. Design domain for the short cantilever fully clamped along the left edge loaded at the centre of the free end.

(triangular shape version) to complex geometries such as the deformed shapes associated with buckling modes.

### 2.1. Spurious modes

A spurious mode is a buckling mode where the displacements corresponding to nodes connected to non-void elements are all zero. A common problem in topology optimization which considers the effect of buckling is the appearance of spurious modes in the void regions. There are five common solutions that can be used to resolve this issue:

- 1) Modifying the stresses of the void elements. Neves et al. (2002) [29] set artificially to zero all stresses in the elements with a volume fraction below a certain threshold.
- 2) Modifying the stiffness of the void elements. Neves et al. (1995) [30] ignored the stress stiffness matrices of elements in void regions. This cut-off method can produce oscillations in the optimization process, which in turn can lead to convergence difficulties. Bendsøe and Sigmund (2004) [31] proposed the use of different penalty schemes for element stiffness matrices and stress stiffness matrices.
- 3) Removing completely the void elements, except for void elements located on the border of the structure. These elements are necessary for the optimization algorithm to grow a structure into the void. Otherwise, this method can produce erroneous solutions (Pedersen (2000) [32]).
- 4) Element removal with reintroduction: originally proposed by Bruns and Tortorelli (2003) [33] and enhanced by Behrou et al. (2021) [34] where void elements are removed from the analysis, and artificial nodal boundary conditions are added to suppress the degrees of freedom surrounded by these elements. The material may be reintroduced into the domain of removed elements, freeing degrees of freedom that were temporarily constrained.
- 5) Pseudo buckling modes identification. Pseudo modes have two important characteristics: 1) Eigenvalues with values close to zero, or alternatively considerably smaller than those of the real modes; 2) The deformation mainly occurs in low-density regions. Therefore, the modal strain energy in low-density regions has a major contribution to the total modal strain energy. Based on the second characteristic, Gao and Ma (2015) [27] proposed to divide the modal strain energy of a mode into two parts, one from the low-density regions and the other from the rest of the structure. When the modal strain energy of low-density regions is greater than a threshold value, the corresponding mode is considered a pseudo mode; otherwise, the mode is treated as real.

From these five common solutions to the issue of identifying spurious modes, the work of Gao and Ma (2015) [27] was implemented in this work and consists of comparing the strain energy of the void region ( $SE_v$ ) with that of the real region ( $SE_r$ ) multiplied by the threshold spurious parameter  $\delta_{sp}$  (Eq. (2)). If the comparison is greater or equal, the mode is

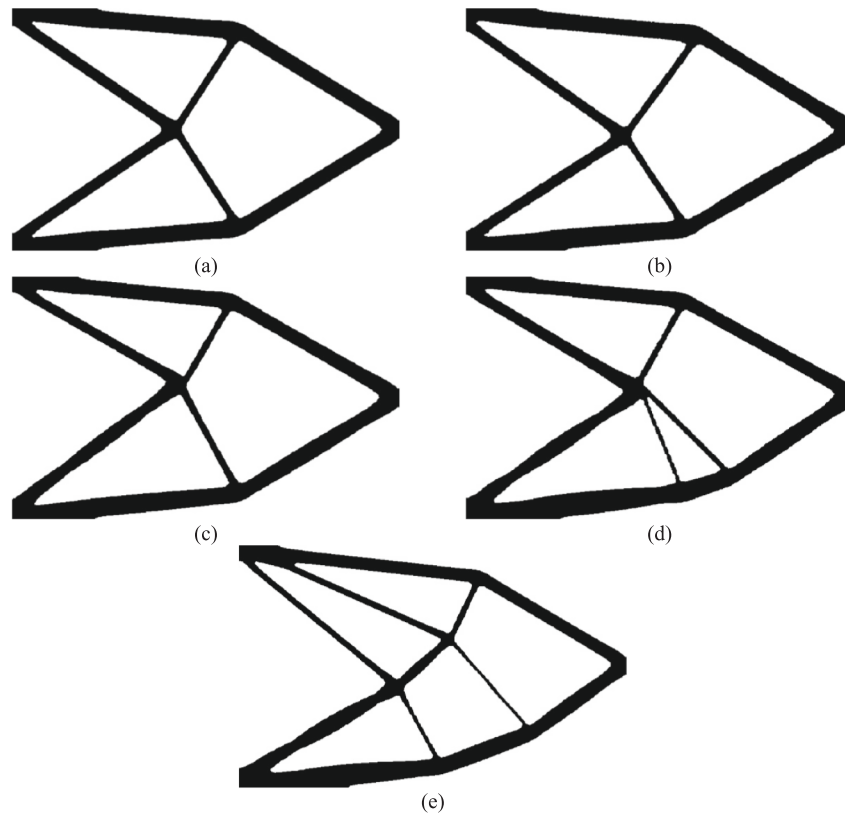


Fig. 12. Final optimal designs for the short cantilever with a final volume fraction of  $V_f/V_0 = 0.2$ , showing the effect of different  $d_r$  values on the optimal design: (a) 0, (b) 0.005, (c) 0.01, (d) 0.015, (e) 0.02.

defined as spurious and therefore disregarded.

$$SE_v \geq \delta_{sp} \times SE_r \tag{2}$$

$$SE_v = \sum SE_o^e$$

$$SE_r = \sum SE_{i,b}^e$$

where  $SE_v$  and  $SE_r$  are the strain energy of the void and real regions,  $SE_o^e$  (out element strain energy),  $SE_{i,b}^e$  (in/boundary element strain energy), and  $\delta_{sp}$  is the threshold spurious parameter with a value between 0 and 1.

### 3. Topology design of continuum structures incorporating buckling effects

The topology design of structures is very often based only on strength and/or stiffness considerations. However, a structure may become unstable before the strength and stiffness criteria are violated.

#### 3.1. Linear and non-linear buckling analysis

Linear buckling of structural members is the most straightforward form of buckling analysis. One major drawback of linear buckling analysis is that no information is obtained on the behaviour of the structure. For more accurate critical load estimates, a non-linear analysis is required [21]. However, the simplicity and lower computational cost of buckling eigenvalue analysis remains relevant in the preliminary stages of the design of a structure [20,21]. Consequently, in most BTO literature, linear buckling analysis is used to generate optimal designs [16, 17, 18, 19, 21, 22, 27, Ferrari and Sigmund (2019) [35]].

#### 3.2. Linear buckling analysis

The linear buckling analysis is governed by the eigenvalue problem of Eq. (3)

$$(\mathbf{K} + \lambda_j \mathbf{K}_\sigma) \mathbf{u}_j = 0 (j = 1, \dots, J) \tag{3}$$

where  $\mathbf{K}$  is the elastic stiffness matrix,  $\mathbf{K}_\sigma$  is the stress stiffness matrix,  $J$  is the number of buckling modes to extract,  $\lambda_j$  is the  $j$ -th eigenvalue and  $\mathbf{u}_j$  is the  $j$ -th displacement eigenvector.

The total number of eigenpairs to extract was determined by Eq. (4)

$$J = \max(j_{ns} + 3, \text{nearest}_{int}(1.25 \times j_{ns})) \tag{4}$$

where ns means non-spurious,  $j_{ns}$  is the first  $j$ -th non-spurious mode. The initial value of  $j_{ns} = 1$  is assumed.

In this work, the ANSYS program [28] was used to carry out the linear buckling analysis. From a structural engineer's perspective, the first lowest non-spurious eigenpair  $(\lambda_{j_{ns}}, \mathbf{u}_{j_{ns}})$  is the critical mode, and therefore this was used to drive the design process. The ANSYS eigensolver used for mode extraction [28] consists of a subspace method with auto-shift technique to improve the accuracy, robustness, and efficiency of the algorithm (Wilson and Itoh (1983) [36]).

#### 3.3. New approach to incorporate buckling effect into the design of 2D continuum structures using the ITD algorithm

To incorporate the buckling effect into the design of 2D continuum structures, the buckling topology design problem is transformed into a stress topology design problem using the shape of the buckling mode of the structure obtained by eigenvalue analysis at each iteration. To achieve this, a linear buckling analysis of the structure (Fig. 1a) is carried out to determine the critical load ( $P_{cr,1}$ ) and its associated mode

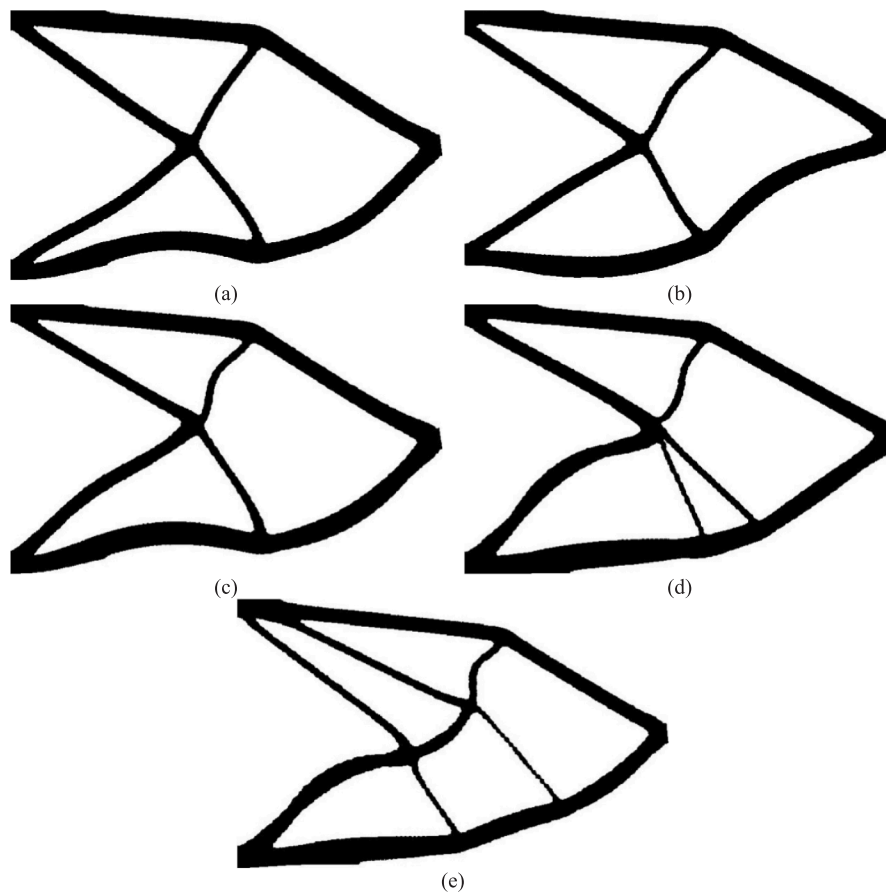


Fig. 13. First lowest buckling mode shapes for the optimal cantilevers of Fig. 12 with  $d_r$  values of: (a) 0, (b) 0.005, (c) 0.01, (d) 0.015, (e) 0.02.

Table 3

Comparison of the first eigenvalue ( $\lambda_1$ ), maximum total displacement ( $d_{t,max}$ ) and compliance ( $C$ ) values for the optimal short cantilever obtained for a volume fraction of  $V_f/V_0 = 0.2$  and different  $d_r$  values.

ANSYS	Eigenvalue analysis	Static analysis	
$d_r$	$\lambda_1$	$d_{t,max}$ (mm)	$C$ (MNmm)
Initial	32.04	11.06	5.528
0.000	1.771	38.26	19.13
0.005	2.049	38.68	19.34
0.010	2.079	39.58	19.79
0.015	2.649	39.98	19.99
0.020	3.124	40.05	20.02

shape, represented by the mode shape displacement vector ( $d_n$ ) in Fig. 1b. The coordinates of the original structure are then modified by the product of a displacement factor ( $d_r$ ) with the mode shape displacement vector ( $d_n$ ), (Fig. 1c). In a 2D continuum, the mode shape can be either as calculated or in the opposite direction, as these are interchangeable. This then requires the coordinates of the original structure to be modified twice, using both of these instances of the mode shape. To these two slightly different structures, the first critical buckling load is applied so that topology optimization can then be carried out. This is achieved in the ITD algorithm by overlaying the criterion distribution obtained from the static analyses, which is analogous to the AND/OR operator applied by Xie and Steven (1994) [37], Young et al. (1999) [38], or Victoria et al. (2010) [39].

The criterion used by ITD algorithm [23] for topology optimization is the von Mises stress ( $\sigma_{vM}$ ), which for a 2D continuum domain is calculated using Eq. (5).

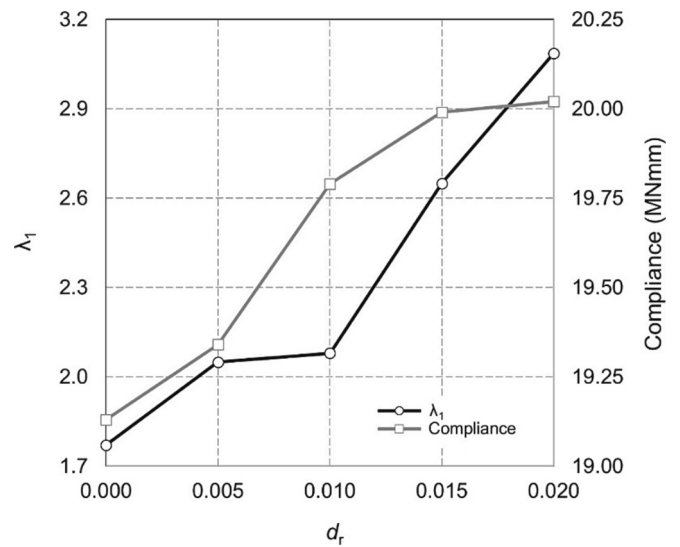


Fig. 14. First eigenvalue and compliance versus displacement factor ratio for the optimal short cantilevers.

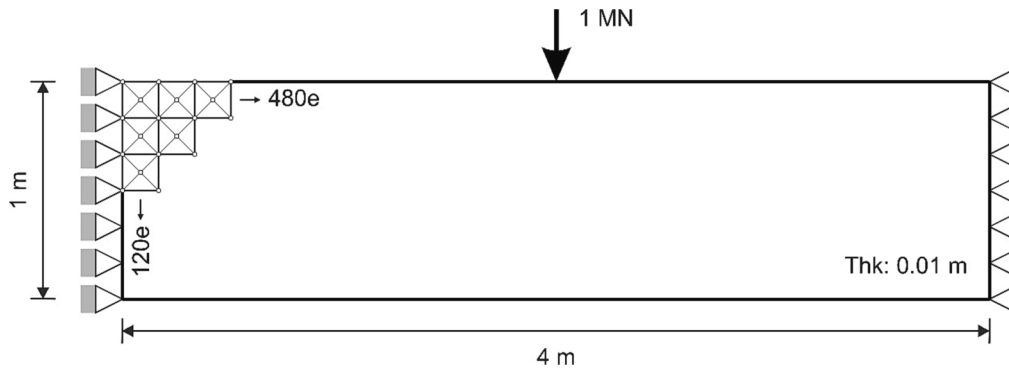


Fig. 15. Design domain for the beam clamped at the two vertical edges and loaded at the centre of the top edge.

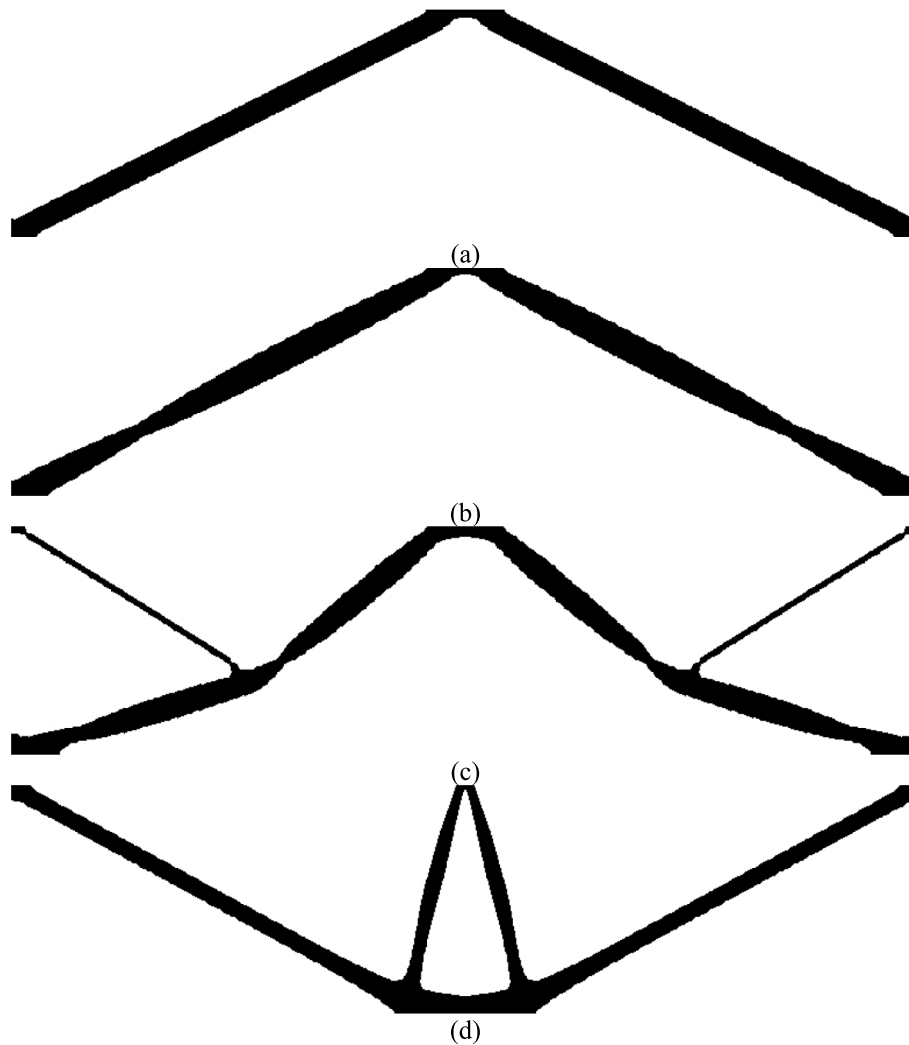


Fig. 16. Clamped beam final designs for a volume fraction of  $V_f/V_0 = 0.1$ . Effect of different  $d_r$  values on the optimal design: (a) 0, (b) 0.01, (c) 0.02, (d) 0.04.

$$\sigma_{vM} = \sqrt{\sigma_x^2 + \sigma_y^2 - \sigma_x\sigma_y + 3\tau_{xy}^2} \quad (5)$$

where  $\sigma_x$ ,  $\sigma_y$ , and  $\tau_{xy}$  are the normal and shear stresses, respectively.

### 3.4. Determining the coordinates of the modified structure from the buckling mode shape

To include the buckling effect in the topology design process using

the ITD algorithm, the modification vector ( $\mathbf{d}$ ) is calculated using Eq. (6). Two modified structural geometries are then generated by firstly adding the modification vector ( $\mathbf{d}$ ) and then its negative ( $-\mathbf{d}$ ) to the coordinates of the nodes of the finite element mesh that represent the structure using Eq. (7).

$$\mathbf{d} = \mathbf{d}_n \times d_r \times \max(L, H) \quad (6)$$

$$\mathbf{X}_{Mod} = \mathbf{X}_{Org} \pm \mathbf{d} \quad (7)$$

**Table 4**

Comparison of the first eigenvalue ( $\lambda_1$ ), maximum total displacement ( $d_{t,max}$ ) and compliance ( $C$ ) values for the optimal beams obtained for a volume fraction of  $V_f/V_0 = 0.1$  and different  $d_r$  values.

ANSYS	Eigenvalue analysis		Static analysis	
	$\lambda_1$	$d_{t,max}$ (mm)	$d_{t,max}$ (mm)	$C$ (MNmm)
$d_r$				
Initial	259.5	3.531	3.531	1.765
0.000	0.817	25.62	25.62	12.81
0.010	1.128	25.75	25.75	12.87
0.020	1.636	32.33	32.33	16.16
0.040	4.036	38.44	38.44	19.22

where  $d_n$  is the normalized displacement vector of the buckling mode shape with a maximum magnitude of 1,  $d_r$  is the displacement factor,  $L$  (length) and  $H$  (height) are the largest horizontal ( $L$ ) and vertical ( $H$ ) dimensions of the design domain,  $X_{Org}$  are the original coordinates of the FE mesh representing the structure and  $X_{Mod}$  are the new modified coordinates of the FE mesh representing the two modified structures.

A schematic representation of the procedure to generate the two modified structural domains is given in Fig. 2. It shows how this is achieved for the  $i^{th}$  node of a simple rectangular beam which for

simplicity is modelled using eight finite elements.

#### 4. The ITD algorithm incorporating buckling effect

The procedure for implementing into the ITD algorithm [23] buckling effect consists of solving a problem of maximizing the critical load for a given volume by a sequence of topology design problems until the desired final volume is reached. In each iteration, the buckling problem is transformed into a stress topology design problem.

In the ITD algorithm, the topology and shape of the design changes iteratively, by continually adding and removing (where the criterion distribution is less than the minimum criterion level) material depending on the shape and distribution of the contour isolines of the required structural behaviour.

The ITD algorithm to incorporate buckling effect into the topology design of 2D continuum consists of the following 11 steps. A schematic representation is given in Fig. 3.

- (1) Define the structure characteristics: geometry, design and non-design domains, material properties, loads and supports.
- (2) Specify the fixed grid mesh: number of finite elements, element type, and fixed grid ratio.

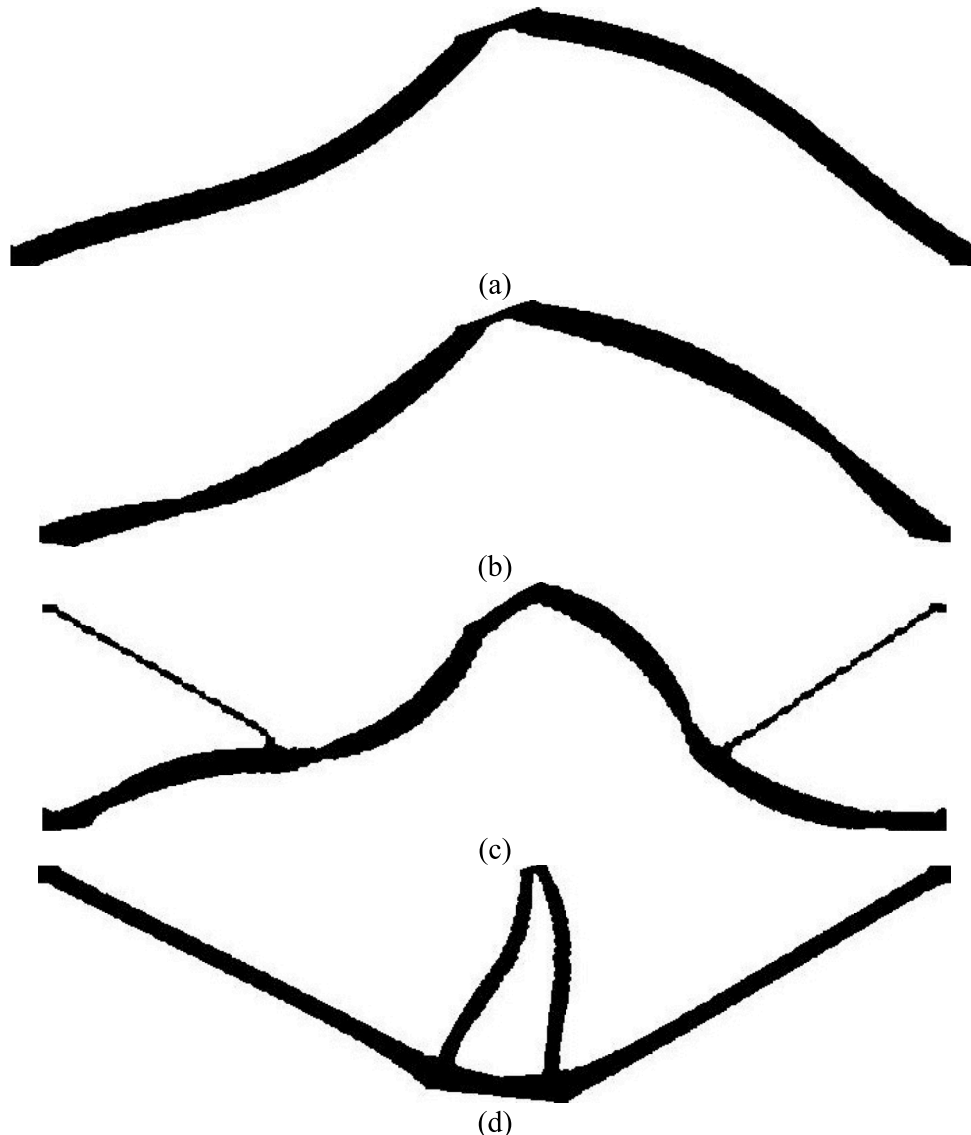


**Fig. 17.** First lowest buckling mode shapes for the optimal beams obtained with  $d_r$  values: (a) 0, (b) 0.01, (c) 0.02, (d) 0.04.

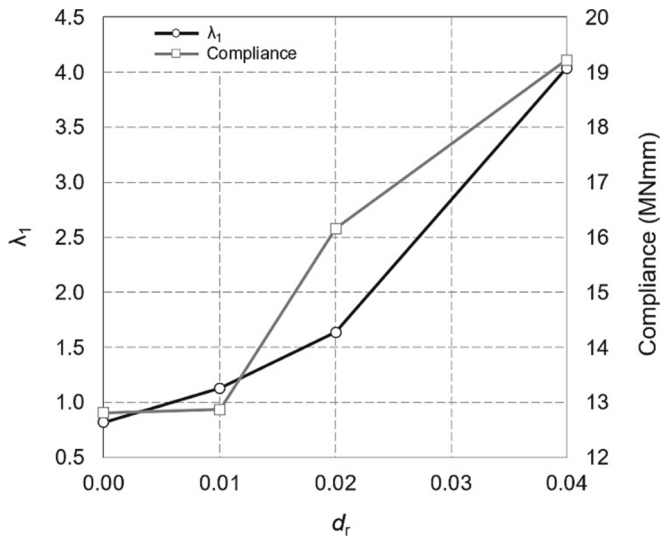


Fig. 18. First eigenvalue and compliance versus displacement factor ratio for the optimal clamped beams.

- (3) Specify the optimization parameters: final design volume ( $V_f$ ), total number of iterations ( $n_i$ ), and displacement factor ratio ( $d_r$ ).
- (4) Carry out a static analysis.
- (5) Carry out an eigenvalue buckling analysis.
- (6) Select the first lowest non-spurious buckling mode, calculate the modification vector ( $d$ ) using Eq. (6) and using Eq. (7) generate the two modified structural geometries.
- (7) Carry out a static FEA for each of the modified structural geometries  $X_{Mod}^{(d)}$  and  $X_{Mod}^{(-d)}$ . Calculate the criterion distribution (von Mises stress in this work), for both cases ( $\sigma_d$  and  $\sigma_{-d}$ , respectively).
- (8) Overlay the resulting von Mises stress distributions from the two modified structural geometries using Eq. (8).

$$\sigma = \max(\sigma_d, \sigma_{-d}) \tag{8}$$

- (9) Determine the target volume using Eq. (9), where  $V_i$  is the design volume in the  $i^{th}$  iteration.

$$V_i = V_{i-1} \left( \frac{n_i - i}{n_i} \right) + V_f \left( \frac{i}{n_i} \right) \tag{9}$$

- (10) Carry out topology optimization of the overlaid von Mises stress distribution ( $\sigma$ ) for the target volume ( $V_i$ ).
- (11) If the total number of iterations has been reached, stop the design process, otherwise, increment the iteration number by 1 and go to step 3.

### 5. Examples

To demonstrate the ability of the ITD algorithm to incorporate the buckling effect, three examples were studied and are presented here, these are the: (1) clamped column loaded in compression at the centre of the top edge; (2) short cantilever loaded in bending at the centre of the free end; and (3) clamped beam loaded at the centre of the top edge. For these examples, the ANSYS program [28] FE were used, specifically the degenerated triangular shape option (by collapsing an element edge) of the four-node plane stress quadrilateral element with two degrees of freedom in each node and four Gauss points. The elasticity modulus was 210 GPa, the Poisson's ratio was 0.3, the fixed grid ratio used was  $r_{fg} = 10^{-4}$ , and the applied force value was chosen so that the first eigenvalue was in the range of  $0 < \lambda_1 < 5$  for the optimal designs. In all

computations  $\lambda_{jns} > 0$  was specified and the threshold spurious parameter was set to  $\delta_{sp} = 0.5$ .

#### 5.1. Clamped column loaded in compression at the centre of the top edge

The dimensions of the column of Fig. 4, are 6 m high, 1 m wide, and 0.01 m thick. The design domain was divided into  $480 \times 80$  quadrilateral-shaped areas. To prevent excessive deformation of finite elements, each area was sub-divided using four triangular finite elements by introducing a node at the centroid of the area, generating a total FE mesh of  $1920 \times 320$  elements. A vertical force of 2 MN was applied at the centre of the top edge in the downward direction and the column was fully clamped along the bottom edge. The final volume fraction was set to be  $V_f/V_0 = 0.5$ . To identify which values of the displacement factor ratios  $d_r$  to use, the following ten values were investigated:  $d_r = 0, 0.01, 0.025, 0.05, 0.1, 0.125, 0.15, 0.2, 0.25, 0.3$ .

Fig. 5 shows the resulting final designs for each value of the displacement factor ratio  $d_r$ . When buckling is not considered ( $d_r = 0$ ), the optimal design is a column with a uniform cross-section (Fig. 5(a)). For values of  $d_r > 0$  (Fig. 5(b) to 5(j)), in addition to the axial (compression) stress, bending stresses are induced, which as they increase with increasing values of  $d_r$ , have the effect of generating a more complex bracing system. Fig. 6 shows the first lowest buckling mode shape for the final designs of the columns represented in Fig. 5 obtained with the ANSYS buckling solver.

Table 1 lists the first eigenvalue obtained by the eigenvalue analysis, and the maximum total displacement and the compliance obtained by the ANSYS static analysis when the optimal columns (Fig. 5) are subjected to the applied force from Fig. 4.

The optimum design when buckling is not considered is given in Table 1 corresponding to Fig. 5(a) ( $d_r = 0$ ) and clearly shows that it is the least stable design with all the material distributed along the load transfer path. As the value of the displacement factor ratio is increased, the level of structural stability increases. For the cases of  $d_r = 0.125, 0.15, 0.2, 0.25, 0.3$  (Fig. 5(f) to 5(j)) a greater fraction of material is distributed in the form of internal bracings, which makes it possible to increase the buckling load value without considerably increasing the value of the maximum total displacement and the compliance.

The evolution of the first eigenvalue and the compliance versus displacement factor ratio for the optimal columns is shown in Fig. 7.

As can be seen in Fig. 7, when the displacement factor ratio is increased the eigenvalue and compliance are also increased.

In the range of  $0 \leq d_r \leq 0.05$  the eigenvalue increases rapidly. In the range  $0.05 \leq d_r \leq 0.15$  the increase is more progressively and for values greater than  $d_r \geq 0.15$  the eigenvalue converges smoothly. The compliance always increases and more rapidly for  $d_r \geq 0.15$ . From these results, it is clear that there is a direct link between increasing the first eigenvalue and also increasing the compliance of the structure. So similarly to the conclusion reached by Gao et al. (2017) [18], the optimal design requires a fine balance between the stiffness (inverse of compliance) and stability (critical load) requirements of the structure.

The results from this work are compared with two equivalent examples from the literature, the 6 by 1 column of Luo and Tong (2015) [17], Fig. 8(a) and the 2 by 1 column of Ferrari et al. (2021) [22], Fig. 8 (b). The finite element used was the four-node plane stress quadrilateral-shaped element with two degrees of freedom in each node and four Gauss points.

The column [17] is 600 mm high, 100 mm wide and 4 mm thick, it was divided using a  $240 \times 40$  FE mesh with  $E = 70\text{GPa}$ , Poisson's ratio  $\nu = 0.3$ ,  $r_{fg} = 10^{-9}$  and  $V_f/V_0 = 0.5$ . A vertical concentrated force of 30 kN was applied at the centre of the top edge. The column [22] is 2 units high, 1 unit wide and 1 unit thick, it was divided using a  $480 \times 240$  FE mesh with  $E = 1$ ,  $r_{fg} = 10^{-6}$  and  $V_f/V_0 = 0.25$ . A distributed load of  $1 \times 10^{-3}$  along a 1/15 length was applied at the centre of the top edge. Both columns were fully clamped along the bottom edges. For both examples,

the displacement factor ratio  $d_r = 0.3$  was used.

Fig. 9 shows the resulting topologies for the 6 by 1 (Fig. 9(a)) and 2 by 1 (Fig. 9(b)) columns resulting from this work. Note that, the topology shown in Fig. 9(b) was obtained by starting with the initial design volume fraction of  $V_f/V_0 = 0.3$  shown as the shaded section in Fig. 8(b) and maximizing the critical load to achieve a final volume fraction of  $V_f/V_0 = 0.25$ .

Fig. 10 shows the first lowest buckling mode shape for the final design of the columns of Fig. 9, these were obtained using the ANSYS buckling solver.

The first eigenvalues corresponding to the optimal columns from Fig. 9(a) and 9(b) are given in Table 2.

The resulting designs generated from this work are in good agreement with those obtained by [17,22] with differences in the value of the first eigenvalue (Table 2) less than 3.5% for the 6 by 1 and 1.5% for the 2 by 1 columns.

### 5.2. Short cantilever loaded in bending at the centre of the free end

The dimensions of the short cantilever of Fig. 11, are 1.6 m long, 1 m high and 0.01 m thick. The design domain was divided into  $96 \times 60$  quadrilateral-shaped areas with each area sub-divided using four triangular finite elements by introducing a node at the centroid of the area, generating a total FE mesh of  $384 \times 240$  elements. A vertical force of 1 MN was applied at the centre of the free end in the downward direction and the cantilever was fully clamped along the left edge. The final volume fraction was set to be  $V_f/V_0 = 0.2$  so that buckling was prominent in the solution. To identify which values of the displacement factor ratios  $d_r$  to use, five values of displacement factor ratio were investigated:  $d_r = 0, 0.005, 0.01, 0.015, 0.02$ .

Fig. 12 shows the resulting designs for each value of the displacement factor ratio  $d_r$ . Fig. 12(a) corresponds with the optimal design with no buckling effect ( $d_r = 0$ ). The topology consists of a symmetrical eight-bar truss design. As  $d_r$  is slightly increased  $d_r = 0.005$ , Fig. 12(b), and  $d_r = 0.01$ , Fig. 12(c) similar topologies are obtained. When  $d_r$  reaches the value of  $d_r = 0.015$ , Fig. 12(d) there is a slight change in the topology as a thinner tension bar is replaced by two bars with a fork-shape, which reduce the length of the external bars acting in compression. Fig. 12(e) shows the optimal design for  $d_r = 0.02$ . The topology changed considerably and suggests a non-symmetrical twelve-bar truss design, with two chains of three bars under compression and three chains of two bars under tension. The bars in compression are shorter and wider with varying cross section that those in tension.

Fig. 13 shows the first lowest buckling mode shape for the final design of the short cantilevers of Fig. 12, these were obtained using the ANSYS buckling solver.

Table 3 lists the first eigenvalue obtained using the eigenvalue analysis, and the maximum total displacement and the compliance obtained using the ANSYS static analysis when the optimal short cantilevers (Fig. 12) are subjected to the applied force from Fig. 11.

Compared with the optimal design with no buckling effect ( $d_r = 0$ ), Fig. 12(a), the major topology changes seen in Fig. 12(d) and 12(e) reduce the buckling length of the longer compression bars increasing the eigenvalue by 49.6% and 76.4%, although the compliance is only increased by 4.5% and 4.68%.

The evolution of the first eigenvalue and the compliance versus displacement factor ratio for the optimal short cantilevers is shown in Fig. 14, where it can be observed that as the displacement factor ratio is increased the eigenvalue and compliance also increase. The eigenvalue increases and more rapidly for  $d_r \geq 0.01$ . The compliance increases rapidly for  $d_r \leq 0.01$  and converges gradually by  $d_r = 0.02$  due to the significant change in the topology of the design.

### 5.3. Clamped beam loaded at the centre of the top edge

The dimensions of the clamped beam of Fig. 15, are 4 m long, 1 m

high, and 0.01 m thick. The design domain was divided into  $120 \times 30$  quadrilateral-shaped areas with each area sub-divided using four triangular finite elements by introducing a node at the centroid of the area, generating a total FE mesh of  $480 \times 120$  elements. A vertical force of 1 MN was applied at the centre of the top edge in the downward direction and the beam was fully clamped at the two vertical edges. The final volume fraction was set to be  $V_f/V_0 = 0.1$ . To identify which values of the displacement factor ratios  $d_r$  to use, these four values were investigated:  $d_r = 0, 0.01, 0.02, 0.04$

Fig. 16 shows the resulting designs for each value of the displacement factor ratio  $d_r$  with Table 4 listing the first eigenvalue obtained by the eigenvalue analysis, the maximum total displacement and the compliance obtained by the static analysis when the optimal beams of Fig. 16 are subjected to the applied force from Fig. 15.

Fig. 17 shows the first lowest buckling mode shape for the final designs of the clamped beam loaded at the centre of the top edge of Fig. 16, these were obtained using the ANSYS buckling solver.

Fig. 16(a) corresponds with the optimal design with no buckling effect ( $d_r = 0$ ) and is the classic solution with two slender bars of uniform cross-section in compression connected to the lower corners. As  $d_r$  is increased to  $d_r = 0.01$ , Fig. 16(b), the topology is similar to Fig. 16(a), but with a non-uniform cross-section. Increasing  $d_r$  further to  $d_r = 0.02$ , results in the topology of Fig. 16(c) which has a slight change as the optimal design continues to have two bars in compression but two thin bars in tension were introduced to reduce the buckling length of the compressed members. In Fig. 16(d) ( $d_r = 0.04$ ) the optimal topology changes completely and the resulting design consists of two long bars in tension of uniform cross-section with two shorter bars in compression of variable cross-section that connects to the applied force. The optimal designs of Fig. 16(c) and 16(d) have similar topologies as those obtained in Ramm et al. (2000) [40], Ramm and Kemmler (2002) [41] and [14]. As was the case in the previous two examples, when the displacement factor ratio increases, the eigenvalue and compliance increase, Fig. 18. Note that compared with the results for the topology of Fig. 16(c), the major topology change seen in Fig. 16(d) correspond with a considerable increase in the eigenvalue by 146.7% but with a slight increase in the compliance by 18.9% (Table 4).

## 6. Conclusions

This paper presents an extension of the isolines topology design (ITD) algorithm of Victoria et al. (2009) [23], by incorporating a new approach that incorporates buckling effect into the design of 2D continuum structures. The approach consists of transforming the buckling topology design problem into a stress-based (von Mises) design problem at each iteration using the shape of the buckling mode of the structure obtained by the eigenvalue analysis. Three examples are presented to show the viability and effectiveness of incorporating this approach into the ITD algorithm. From the results obtained, three conclusions can be made: (1) The ITD algorithm was successfully extended to incorporate linear buckling effect using the new approach. The results from the examples presented were in good agreement with those from the literature; (2) Increasing the displacement factor ratio ( $d_r$ ) increases the magnitude of the critical buckling load but has a less significant effect on the stiffness of the resulting designs; (3) The value of the displacement factor ratio  $d_r$  to use depends on two factors: (i) The predisposition of the structure to buckle and (ii) the elastic modulus of material used. Based on the examples used in this study, for case (i), if the structure has a high pre-disposition to buckle, typical values of  $d_r$  to use are in the range  $d_r = 0.01 - 0.05$ . If the structure has a moderate predisposition to buckle typical values of  $d_r$  to use are in the range  $d_r = 0.01 - 0.1$ . And for structures with a moderate predisposition to buckle typical values of  $d_r$  to use are in the range  $d_r = 0.01 - 0.3$ . For case (ii), since the elastic modulus affects both the stiffness of the structure and its ability to withstand buckling, using significantly different values of the elastic modulus will require different values of  $d_r$ . As a rule of thumb, for values

of the elastic modulus significantly lower than those presented in this paper, will require lower values of  $d_i$  in the range  $d_i \leq 0.01$ .

### Declaration of Competing Interest

The authors declare that they have no known competing financial interests or personal relationships that could have appeared to influence the work reported in this paper.

### Acknowledgments

The authors would like to thank the reviewers of this paper for their invaluable advice in ways to improve the article.

#### Funding.

This research did not receive any specific grant from funding agencies in the public, commercial, or not-for-profit sectors. The article publishing charge was support by the Technical University of Cartagena. Its support is greatly appreciated.

### References

- Ooms T, Vantghem G, Thienpont T, Van Coile R, De Corte W. Compliance-based topology optimization of structural components subjected to thermo-mechanical loading. *Struct Multidiscip Optim* 2023;66:126. <https://doi.org/10.1007/s00158-023-03563-3>.
- L. Wang, X. Zhao, Z. Wu, W. Chen, Evidence theory-based reliability optimization for cross-scale topological structures with global stress, local displacement, and micro-manufacturing constraints. *Struct. Multidiscip. Optim.* (2022) 65–23, 10.1007/s00158-021-03112-w.
- Zhang Y, Gao L, Xiao M. Maximizing natural frequencies of inhomogeneous cellular structures by Kriging-assisted multiscale topology optimization. *Comput Struct* 2020;230:106197. <https://doi.org/10.1016/j.compstruc.2019.106197>.
- Hajlaoui A, Chebbi E, Dammak F. Three-dimensional thermal buckling analysis of functionally graded material structures using a modified FSDT-based solid-shell element. *Int J Press Vessel Pip* 2021;194:104547. <https://doi.org/10.1016/j.ijpvp.2021.104547>.
- Liang K, Li Z. The reformulated Koiter-Newton method for thermal-mechanical buckling and postbuckling analysis of thin-walled structures. *Internat J Numer Methods Eng* 2022;123:1933–53. <https://doi.org/10.1002/nme.6922>.
- Ngoc NM, Hoang V-N, Lee D. Concurrent topology optimization of coated structure for non-homogeneous materials under buckling criteria. *Eng Comput* 2022. <https://doi.org/10.1007/s00366-022-01718-2>.
- Guo L, Wang X, Meng Z, Yu B. Reliability-based topology optimization of continuum structure under buckling and compliance constraints. *Internat J Numer Methods Eng* 2022. <https://doi.org/10.1002/nme.6997>.
- Jiang Y, Zhan K, Xia J, Zhao M. Topology Optimization for Minimum Compliance with Material Volume and Buckling Constraints under Design-Dependent Loads. *Appl Sci* 2023;13:646. <https://doi.org/10.3390/app13010646>.
- Ebeling-Rump M, Hömberg D, Lasarzik R, Petzold T. Topology optimization subject to additive manufacturing constraints. *J Math Industry* 2021;11:19. <https://doi.org/10.1186/s13362-021-00115-6>.
- Li Z, Wang L, Luo Z. A feature-driven robust topology optimization strategy considering movable non-design domain and complex uncertainty. *Comput Methods Appl Mech Engrg* 2022;401:115658.
- Li Z, Wang L, Lv T. A level set driven concurrent reliability-based topology optimization (LS-CRBTO) strategy considering hybrid uncertainty inputs and damage defects updating. *Comput Methods Appl Mech Engrg* 2023;405:115872. <https://doi.org/10.1016/j.cma.2022.115872>.
- Rozvany GIN. Difficulties in Truss Topology Optimization with Stress, Local Buckling and System Stability Constraints. *Struct Optim* 1996;11:213–7. <https://doi.org/10.1007/BF01197036>.
- Rahmatalla S, Swan CC. Form Finding of Sparse Structures with Continuum Topology Optimization. *J Struct Eng* 2003;129(12):1707–16. [https://doi.org/10.1061/\(ASCE\)0733-9445\(2003\)129:12\(1707\)](https://doi.org/10.1061/(ASCE)0733-9445(2003)129:12(1707)).
- Kemmler R, Lipka A, Ramm E. Large Deformations and Stability in Topology Optimization. *Struct Multidiscip Optim* 2005;30:459–76. <https://doi.org/10.1007/s00158-005-0534-0>.
- Browne PA, Budd CJ, Gould NIM, Kim HA, Scott JA. A fast Method for Binary Programming using First-order Derivatives, with Application to Topology Optimization with Buckling Constraints. *Int J Numer Meth Eng* 2012;92(12): 1026–43. <https://doi.org/10.1002/nme.4367>.
- Bochenek B, Tajs-Zielińska K. Minimal Compliance Topologies for Maximal Buckling Load. *Struct Multidiscip Optim* 2015;51:1149–57. <https://doi.org/10.1007/s00158-014-1202-z>.
- Luo Q, Tong L. Structural Topology Optimization for Maximum Linear Buckling Loads by using a Moving Iso-Surface Threshold Method. *Struct Multidiscip Optim* 2015;52:71–90. <https://doi.org/10.1007/s00158-015-1286-0>.
- Gao X, Li L, Ma H. An Adaptive Continuation Method for Topology Optimization of Continuum Structures Considering Buckling Constraints. *Int J Appl Mech* 2017;9(7):1–24. <https://doi.org/10.1142/S1758825117500922>.
- Ferrari F, Lazarov BS, Sigmund O. Eigenvalue topology optimization via efficient multilevel solution of the frequency response. *Int J Numer Meth Eng* 2018;115: 872–92. <https://doi.org/10.1002/nme.5829>.
- Townsend S, Kim HA. A Level Set Topology Optimization Method for the Buckling of Shell Structures. *Struct Multidiscip Optim* 2019;60:1783–800. <https://doi.org/10.1007/s00158-019-02374-9>.
- Dalkint A, Wallin M, Tortorelli DA. Structural stability and artificial buckling modes in topology optimization. *Struct Multidiscip Optim* 2021;64:1751–63. <https://doi.org/10.1007/s00158-021-03012-z>.
- Ferrari F, Sigmund O, Guest JK. Topology optimization with linearized buckling criteria in 250 lines of Matlab. *Struct Multidiscip Optim* 2021;63:3045–66. <https://doi.org/10.1007/s00158-021-02854-x>.
- Victoria M, Martí P, Querin OM. Topology Design of Two-Dimensional Continuum Structures using Isolines. *Comput Struct* 2009;87(1–2):101–9. <https://doi.org/10.1016/j.compstruc.2008.08.001>.
- García-Ruiz MJ, Steven GP. Fixed Grid Finite Elements in Elasticity Problems. *Eng Comput* 1999;16(2):145–64. <https://doi.org/10.1108/02644409910257430>.
- Zhou M. *Topology Optimization for Shell Structures with Linear Buckling Responses*. WCCM VI: Beijing, China; 2004. p. 5–10.
- Lindgaard E, Dahl J. On compliance and buckling objective functions in topology optimization of snap-through problems. *Struct Multidiscip Optim* 2013;47:409–21. <https://doi.org/10.1007/s00158-012-0832-2>.
- Gao X, Ma H. Topology Optimization of Continuum Structures under Buckling Constraints. *Comput Struct* 2015;157:142–52. <https://doi.org/10.1016/j.compstruc.2015.05.020>.
- Swanson Analysis Systems ANSYS, User's manual, version 19 and theory reference, 2019.
- Neves MM, Sigmund O, Bendsoe MP. Topology Optimization of Periodic Microstructures with a Penalization of Highly Localized Buckling Modes. *Int J Numer Meth Eng* 2002;54(6):809–34. <https://doi.org/10.1002/nme.449>.
- Neves MM, Rodrigues H, Guedes JM. Generalized Topology Design of Structures with a Buckling Load Criterion. *Struct Optim* 1995;10:71–8. <https://doi.org/10.1007/BF01743533>.
- Bendsoe MP, Sigmund O. *Topology optimization: Theory, Methods and Applications*. Berlin. Springer 2004. <https://doi.org/10.1007/978-3-662-05086-6>.
- Pedersen NL. Maximization of Eigenvalues using Topology Optimization. *Struct Multidiscip Optim* 2000;20:2–11. <https://doi.org/10.1007/s001580050130>.
- Bruns TE, Tortorelli DA. An element removal and reintroduction strategy for the topology optimization of structures and compliant mechanisms. *Int J Numer Meth Eng* 2003;57:1413–30. <https://doi.org/10.1002/nme.783>.
- Behrou R, Lotfi R, Carstensen JV, Ferrari F, Guest JK. Revisiting element removal for density-based structural topology optimization with reintroduction by Heaviside projection. *Comput Methods Appl Mech Engrg* 2021;380:113799. <https://doi.org/10.1016/j.cma.2021.113799>.
- Ferrari F, Sigmund O. Revisiting Topology Optimization with Buckling Constraints. *Struct Multidiscip Optim* 2019;59:1401–15. <https://doi.org/10.1007/s00158-019-02253-3>.
- Wilson EL, Itoh T. An Eigensolution Strategy for Large Systems. *Comput Struct* 1983;16(1–4):259–65. [https://doi.org/10.1016/0045-7949\(83\)90166-9](https://doi.org/10.1016/0045-7949(83)90166-9).
- Xie YM, Steven GP. Optimal Design of Multiple Load Case Structures using an Evolutionary Procedure. *Eng Comput* 1994;11(4):295–302. <https://doi.org/10.1108/02644409410799290>.
- Young V, Querin OM, Steven GP. 3D and Multiple Load Case Bi-Directional Evolutionary Structural Optimization (BESO). *Struct Optim* 1999;18:183–92. <https://doi.org/10.1007/BF01195993>.
- Victoria M, Querin OM, Martí P. Topology Design for Multiple Loading Conditions of Continuum Structures using Isolines and Isosurfaces. *Finite Elem Anal Des* 2010; 46(3):229–37. <https://doi.org/10.1016/j.finel.2009.09.003>.
- Ramm E, Schwarz S, Kemmler R. *Advances in Structural Optimization Including Nonlinear Mechanics*. Barcelona, Spain: ECCOMAS; 2000.
- E. Ramm, R. Kemmler, Stability and Large Deformations in Structural Optimization, Proceedings of Int. Symposium on Lightweight Structures in Civil Engineering, Warsaw, Poland, 443–454, 2002.